Obrabotka metallov (tekhnologiya, oborudovanie, instrumenty) = Metal Working and Material Science. 2026 vol. 28 no. 3 pp. 331–344
ISSN: 1994-6309 (print) / 2541-819X (online)
DOI: 10.17212/1994-6309-2026-28.3-331-344

NSTU NETI

Obrabotka metallov -
Metal Working and Material Science

Journal homepage: http://journals.nstu.ru/obrabotka_metallov

Investigation of the effect of additive manufacturing process parameters on the fabrication of a 3D-printed talus bone prototype

Devendra Agrawal [1, a, *], *Sushil Patil* [1, b], *Nitin Ambhore* [2, c], *Dinesh Washimkar* [2, d], *Dhroov Agrawal* [3, e]

[1] Department of Mechanical Engineering, S.V.P.M'S College of Engineering Malegaon (Bk.), SPPU, Pune, 413115, Maharashtra, India
[2] Department of Mechanical Engineering, Vishwakarma Institute of Technology, SPPU, Pune, 411048, Maharashtra, India
[3] Department of Bachelor of Medicine & Bachelor of Surgery, KD Medical College, Mathura, 281401, Uttar Pradesh, India

[a] https://orcid.org/0000-0002-2477-1841, dpagrawal@engg.svpm.org.in; [b] http://orcid.org/0000-0002-0547-6038, sspatil@engg.svpm.org.in;
[c] https://orcid.org/0000-0001-8468-8057, nitin.ambhore@vit.edu; [d] https://orcid.org/ 0000-0002-1312-2619, dinesh.washimkar@vit.edu;
[e] https://orcid.org/0009-0000-8547-9484, dhroovagrawal109@gmail.com

ARTICLE INFO

Article history:
Received: 28 May 2026
Revised: 13 June 2026
Accepted: 14 August 2026
Available online: 15 September 2026

Keywords:
3D printing
Additive manufacturing
Fused deposition modelling
Polylactic acid
Talus bone
Grey relational analysis
Prototype

ABSTRACT

Introduction. Additive manufacturing, and in particular fused deposition modelling (*FDM*), enables the fabrication of geometrically complex parts without dedicated tooling, which is especially valuable for patient-specific biomedical devices. The mechanical performance of polylactic acid (*PLA*) parts, however, depends strongly on the combination of printing parameters, and the available data on the joint influence of layer thickness, nozzle temperature, and material flow rate on the full set of strength characteristics remain fragmentary, which complicates process selection for anatomical prototypes. The aim of this work is to determine the optimum combination of *FDM* printing parameters for *PLA* parts that maximizes the integrated strength response, and to fabricate, using the identified settings, a full-scale patient-specific prototype of the human talus bone from computed tomography data. **Materials and methods.** A *Taguchi L27* orthogonal array was implemented with three levels of layer thickness (0.1–0.3 mm), nozzle temperature (190–210 °C), and material flow rate (95–105%). Tensile strength and *Young's* modulus were determined in accordance with *ASTM D638–22* on a universal testing machine at a crosshead speed of 5 mm/min; specific fracture energy (toughness) was measured according to *ASTM D256–23* using a notched *Izod* pendulum impact tester. The significance of the factors was evaluated by analysis of variance (*ANOVA*), and multi-response optimization was performed by grey relational analysis (*GRA*). The geometry of the fabricated prototype was inspected on a coordinate measuring machine. **Results and discussion.** Material flow rate was found to be the dominant factor for tensile strength (contribution of 50.3 %) and for toughness (92.9%), whereas *Young's* modulus is governed primarily by layer thickness. The highest grey relational grade (0.853) was obtained at a layer thickness of 0.1 mm, a nozzle temperature of 210 °C, and a flow rate of 105%. The dimensional deviations of the fabricated prototype from the *CT* data did not exceed 0.2 mm, which confirms its suitability as a master model for the subsequent manufacture of an implant from a biocompatible material.

For citation: Agrawal D., Patil S., Ambhore N., Washimkar D., Agrawal D. Investigation of the effect of additive manufacturing process parameters on the fabrication of a 3D-printed talus bone prototype. *Obrabotka metallov (tekhnologiya, oborudovanie, instrumenty) = Metal Working and Material Science*, 2026, vol. 28, no. 3, pp. 331–344. DOI: 10.17212/1994-6309-2026-28.3-331-344. (In Russian).

Introduction

Additive manufacturing (*AM*) is a cutting-edge technology that enables the creation of novel shapes and structures previously unattainable using conventional techniques [1–2]. Because manufacturing is layer-by-layer, it is possible to develop intricate shapes without joints. Recently, the medical field has made extensive use of *AM* to meet the demands of patients and physicians. It is used in the manufacturing of surgical and diagnostic medical equipment such as orthoses and prostheses, with a reduction in manufacturing

*** Corresponding author**
Devendra Agrawal, Ph.D. (Engineering), Associate Professor
S.V.P.M'S College of Engineering Malegaon (Bk.),
Savitribai Phule Pune University, Pune,
Maharashtra, India.
Tel.: +91-9421054282, **e-mail**: dpagrawal@engg.svpm.org.in

cost and time. *AM* is effectively used in orthopaedic, dental, prosthetic, and food applications, as well as in textile manufacturing. It also addresses the relationship between *AM* and *Industry 4.0* in the context of sustainability, and it has demonstrated that *AM* holds great promise for opening a new avenue for the creation of customized bone and bone-joint implants compared with traditional methods [3-4]. *AM* is a widely used method in biomedicine because it offers rapid prototyping, on-demand, and cost-effective manufacturing methods, and it is claimed that additively manufactured medical implants can increase precision and safety in medical treatment [1]. The work in [5] investigated the variables that affect bone characteristics, including materials, porosity, and surface modification, as well as mechanical properties. The optimum set of printing parameters for process parameters such as print speed, flow rate, and layer height was obtained with respect to the bioimplant's compressive strength and geometric accuracy using full factorial analysis [6]. The potential of using *PLA–Mg* composite scaffolds that are 3D-printed for use in hard tissue engineering was also explored [7]. The work in [8] explained the effect of *AM* technology on the financial aspect of its applications in the medical sector through the manufacturing of dental and orthopaedic prostheses. The potential of additive manufacturing in biomedical applications is demonstrated with a variety of materials [8–9]. Improvement in process factors such as layer height, nozzle temperature, printing speed, and fill spacing has been observed to affect tensile strength and external dimensions [10]. The optimization of process parameters for print strength parameters such as layer height, print speed, and cell shape was done using the *GRA* approach [11]. The work in [12] adjusted the printing parameters that can be used in the *FDM* manufacturing process to obtain the best printing parameters and the shortest production time for *PLA*. The impact of 3D printing process parameters on the tensile characteristics of continuous carbon fiber-reinforced *PLA* composites was investigated, and *PLA* fatigue behavior under various printing conditions was observed [13–14]. The effects of nozzle temperature (***NT***), printing speed (***PS***), and layer thickness (*LT*) on the specific ultimate tensile strength ($\boldsymbol{S_{uts}}$) and energy consumption ($\boldsymbol{S_{ec}}$) of 3D-printed polyether ether ketone (*PEEK*) parts have been studied [15]. From the above, it is observed that *AM* has inherent advantages including lower equipment and material cost, easy conversion of *CAD* to a part, design freedom (lattice/honeycomb) with rapid prototyping, shorter processing and manufacturing times than traditional machining techniques, and the capacity to create parts with intricate geometries. It has a high strength-to-weight ratio and can make components with the same precision and reproducibility. It also revealed that an important aspect of using additive manufacturing with 3D printing is the use of optimum printing parameters for the required print strength of the responses. A biomedical prototype, i.e., the talus bone, is developed using the optimum set of printing settings.

The talus bone (astragalus) is a small bone in the foot ankle (Fig. 1). The location of the bone is shown in Fig. 2. The talus is the second largest bone in the back of the foot. The talus meets the tibia (shin bone) and fibula (calf bone) to form the ankle joint. The talus bone enables the movement of the foot up and down and also helps to maintain body balance by allowing lateral movement of the foot. It supports and protects the ligaments in the ankle, heel, and foot. The talus is important because it forms the ankle joint. The talus is shaped like a saddle. It has two flared lower ends and a domed ridge in the middle. It is covered in a layer

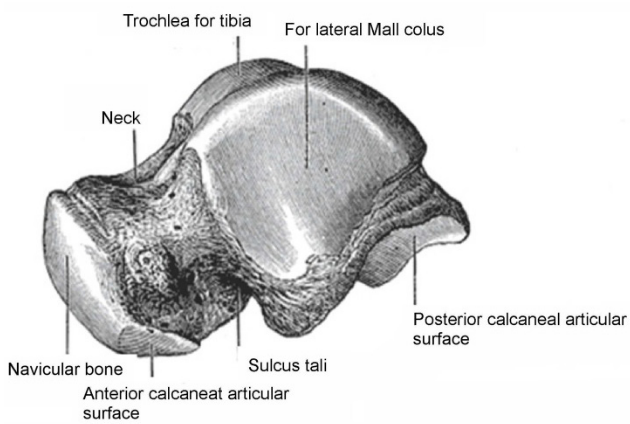

Fig. 1. Morphology of the talus bone

of cartilage that acts as a cushion, shock absorber, and lubricant to help the ankle move smoothly. Unlike many other bones, the talus is not connected to any muscles. It may need surgery to repair the bone or physical therapy to regain strength and mobility once it is broken (fractured). A bone density test (*DEXA* or *DXA* scan) is the most often performed procedure to assess the state of the talus bones. ***The major objective of the work*** is to employ *fused deposition modeling* (*FDM*)-based additive manufacturing to create a patient-specific three-dimensional (3D) prototype of the human talus (astragalus) bone utilizing *STL* data generated from *CT* scans. The study further investigates the influence of key *FDM* process parameters, namely layer height, nozzle temperature, and flow rate, on the mechanical properties of polylactic acid (*PLA*)-printed specimens. The mechanical performance of the fabricated specimens is evaluated in terms of tensile strength, *Young's* modulus, and toughness using relevant standardized testing methods. This study employs grey relational analysis (*GRA*) to optimize the *FDM* printing parameters, thereby identifying the optimal combination of process settings that maximizes the overall mechanical performance of the *PLA* specimens.

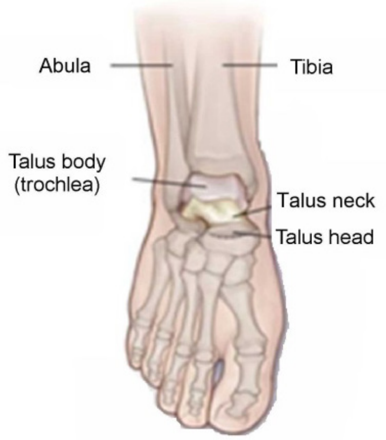

Fig. 2. Anatomical location of the talus bone within the ankle joint

In the current investigation, *AM* using fused deposition modelling is used for the development of a prototype of the human talus bone. The optimal printing parameters, including layer height (mm), nozzle temperature (°C), and flow rate (%) for the *PLA* material's tensile strength (MPa), Young's modulus (GPa), and toughness (J/mm^2), are evaluated using the *GRA* method. The effect of process parameters is investigated during testing. *ANOVA* analysis is used to identify significant process parameters. For biomedical applications such as talus bone printing, the ideal set of printing parameters is utilized. Computed tomography (*CT*) scan data obtained during patient treatment are used to create the software file (*STL* format). The dimensions of the actual size of the adult patient's talus bone and additively manufactured bone are compared in the measurement laboratory. This will be helpful for developing a realistic model of various bone implants and bone joints [16].

Materials and methods

Polylactic acid (*PLA*) is one of the most widely used materials in fused deposition modeling (*FDM*) due to its low cost, easy availability, low melting temperature, good mechanical strength, low warping, and odorless nature. In the *FDM* process, a three-dimensional *CAD* model is converted into an *STL* file, which is then sliced into layers to generate printing instructions for the printer. The object is fabricated layer by layer through material deposition, followed by post-processing, such as vapor finishing to improve the surface finish. Owing to its accuracy and customization capability, *FDM* technology is extensively used in biomedical applications, including orthopaedic, spinal, maxillofacial, neurosurgical, and cardiovascular implant prototyping.

In compliance with *ASTM D256-23: Standard Test Methods for Determining the Izod Pendulum Impact Resistance of Plastics*, an *Izod* pendulum impact testing machine was used to assess the impact toughness of the *FDM*-fabricated *PLA* specimens. Standard notched specimens were prepared in accordance with *ASTM D256-23*. With the notched side facing the pendulum striker, each specimen was positioned vertically as a cantilever beam. The testing apparatus automatically measured the energy absorbed during fracture after the pendulum was released to fracture the specimen in a single strike. By dividing the absorbed impact energy by the cross-sectional area at the notch, the impact strength (toughness) was determined and expressed in J/mm^2. For every experimental condition, five specimens were evaluated, and the average result was reported to ensure repeatability and reliability.

A universal testing machine (*UTM*) was used to assess the tensile properties of the PLA specimens in compliance with *ASTM D638-22: Standard Test Method for Tensile Properties of Plastics*. The stress-strain curve was obtained by recording the applied load and displacement during the tests, which were conducted at a crosshead speed of 5 mm/min. *Young's* modulus was computed from the initial linear elastic region of the stress-strain curve, whereas the ultimate tensile strength was determined from the maximum stress before fracture. The optimum set of printing settings for producing bioimplants like the talus bone is found using the grey relational analysis approach [17]. Layer height (mm), flow rate (%), and nozzle temperature (°C) are crucial factors that affect the strength of the 3D prints. During the design of experiments (*DoE*), each parameter has three levels: low, medium, and high (Table 1).

Table 1

Printing parameters and *DoE* levels

Parameter	Unit	Level 1	Level 2	Level 3
Layer thickness	mm	0.1	0.2	0.3
Nozzle temperature	°C	190	200	210
Flow rate	%	95	100	105

Other printing parameters such as print speed (60 mm/s), bed temperature (60 °C), nozzle gap height (0.1 mm), and retraction distance (1 mm) are kept constant during the process. A design of experiments (*L27* array) with three replicates was performed in the laboratory (Table 2).

Table 2

Orthogonal (L_{27}) data with output responses

Sr. No.	Layer thickness (mm)	Nozzle temperature (°C)	Flow rate (%)	Tensile strength (MPa)	Toughness (J/mm^2)	*Young's* modulus (GPa)
1	0.1	190	95	21	35	2.40
2	0.1	190	100	28	48	2.52
3	0.1	190	105	42	59	2.68
4	0.1	200	95	25	41	2.45
5	0.1	200	100	48	47	2.62
6	0.1	200	105	54	58	2.80
7	0.1	210	95	47	44	2.95
8	0.1	210	100	55	48	3.05
9	0.1	210	105	57	58	3.49
10	0.2	190	95	17	34	3.20
11	0.2	190	100	28	45	3.25
12	0.2	190	105	38	61	3.30
13	0.2	200	95	23	38	3.20
14	0.2	200	100	30	48	3.40
15	0.2	200	105	40	62	3.42
16	0.2	210	95	26	41	3.25
17	0.2	210	100	32	50	3.42
18	0.2	210	105	42	64	3.48
19	0.3	190	95	27	34	3.40
20	0.3	190	100	35	46	3.58
21	0.3	190	105	44	57	3.52
22	0.3	200	95	28	36	3.45
23	0.3	200	100	38	47	3.60
24	0.3	200	105	46	59	2.89
25	0.3	210	95	29	39	3.52
26	0.3	210	100	42	44	2.80
27	0.3	210	105	52	60	2.50

"Larger-the-better" quality characteristics for tensile strength, toughness, and *Young's* modulus are employed in the linear normalization procedure of the original sequence, according to the following equation (Eq. 1) [18]:

$$x_i(k) = \frac{x_i^{(0)}(k) - \min x_i^{(0)}(k)}{\max x_i^{(0)}(k) - \min x_i^{(0)}(k)}. \quad (1)$$

Equation (2) is used for normalizing "smaller-the-better" performance:

$$x_i(k) = \frac{\max x_i^{(0)}(k) - x_i^{(0)}(k)}{\max x_i^{(0)}(k) - \min x_i^{(0)}(k)}, \quad (2)$$

where $x_i^{(0)}(k)$ is the reference sequence; min $x_i^{(0)}(k)$ is the minimum value of $x_i^{(0)}(k)$; max $x_i^{(0)}(k)$ is the maximum value of $x_i^{(0)}(k)$; $x_i(k)$ is the value obtained after grey relation generation.

The deviation sequence is determined using Eq. (3):

$$\Delta 0_i(k) = \left| x_0^{*}(k) - x_i(k) \right|. \quad (3)$$

The deviation sequence $x_i(k)$ is the absolute difference between the reference sequence $x_0^{*}(k)$ and the comparability sequence $x_0^{*}(k)$ after normalization. The value $x_0^{*}(k)$ was considered as 1. The grey relational coefficient (*GRC*) $\gamma(x_0(k), x_i(k)$ that measures the closeness of each response to the ideal performance can be expressed in Eq. (4):

$$\gamma(x_0(k), x_i(k)) = \frac{\Delta \min + \xi \Delta \max}{\Delta 0_i\ (k) + \xi \Delta \max}. \quad (4)$$

The grey relational grade (*GRG*), which combines multiple responses into a single performance index, is shown in Eq. (5):

$$\Gamma(x_0, x_i) = \frac{\sum_{j=1}^{n} \gamma\left(x_0(k), x_i(k)\right)}{j}, \quad (5)$$

where $\Gamma(x_0, x_i)$ is the weighted grey relational grade; *j* is the number of response parameters; $\gamma(x_0(k), x_i(k)$ is the grey relational coefficient (Table 6).

An orthopaedic surgeon provides a *CD* or *DVD* that contains patient *CT* scans from the radiology or medical imaging department. A *CT* scan is performed on the talus to obtain the exact dimensions of the patient. The scanned data are converted into an *STL* file. A file containing commands and code is supplied to the *AM* machine. The process produces a 3D print of the human talus bone accurately.

Results and discussion

The impact of additive manufacturing process parameters on *PLA* was examined. Reduced layer thickness affects print time and cost, but it also improves resolution and possibly the part's mechanical performance. It is observed that when the deposited layer thickness is small (0.1 mm), it improves the intermolecular bonding between two adjacent layers due to a larger surface area in contact. Every layer is compressed and shows better adhesion with the next deposited layer. Tensile strength increases from 21 MPa to 42 MPa with an increase in layer thickness from 0.1 to 0.3 mm.

A further increase in layer thickness (0.2 mm to 0.3 mm) shows a downward trend in tensile strength (MPa). This is attributed to the formation of voids between the two layers during filling of the print. The presence of voids reduces the strength of the print per unit area. An increase in flow rate from 95% to 100% results in strong covalent bonds between the deposited layers with less porosity and fewer voids in between, as well as better fusion of layers, but a further increase in flow rate (100% to 105%) leads to a bulging effect with internal stresses and microcracks during solidification, which results in poor surface quality. The overall effect of material flow rate on strength properties exhibits a parabolic trend. The impact of layer thickness and nozzle temperature on tensile strength is depicted in Fig. 3. Table 3 shows the analysis of variance for tensile strength. It is observed that flow rate is the most significant process parameter for tensile strength (MPa), followed by layer height (mm) and nozzle temperature (°C).

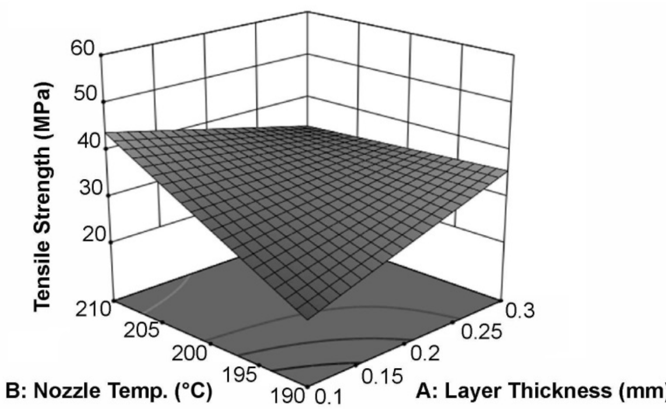

Fig. 3. Tensile strength (MPa) as a function of layer thickness (mm) and nozzle temperature (°C)

Table 3

***ANOVA* results for tensile strength (MPa)**

Source	*DF*	*Seq. SS*	*Adj. MS*	*F*	*P*
Layer thickness	2	582.30	291.15	12.43	0.000
Nozzle temperature	2	578.07	289.04	12.34	0.000
Flow rate	2	1647.19	823.59	35.16	0.000
Error	20	468.00	23.43	–	–
Total	26	3276.00	–	–	–

It is observed that with an increase in nozzle temperature from 190 °C to 210 °C, *Young's* modulus values show an increasing trend, because strong thermal contact allows the layer to fuse fully. The layer interface improves with smooth deposition and minimal porosity. A further increase in nozzle temperature from 200 °C to 210 °C promotes better melting with strong bonding. The material flows smoothly through the nozzle with uniform deposition.

Young's modulus shows an increasing trend with increasing nozzle temperature. However, an increase in flow rate and layer thickness leads to the creation of voids, gaps, and incomplete fusion between deposited layers, which decreases the effective cross-sectional area and weakens interlayer adhesion. *Young's* modulus shows a decreasing trend with increasing flow rate and layer thickness. Fig. 4 shows the effect of flow rate and nozzle temperature on Young's modulus with a parabolic nature. From Table 4, *ANOVA* analysis reflects that layer height is the most prominent parameter for Young's modulus. Nozzle temperature and flow rate have less effect on the *Young's* modulus of the printed part.

To prevent the nozzle from becoming clogged, the filament must be melted at a high enough temperature. The precision of the geometrical dimensions improves with flow rate optimization. Layers may develop voids or gaps if the flow rate is inadequate. This affects layer adhesion and the mechanical properties of the print. Toughness has a combined effect of flow rate, layer thickness, and nozzle temperature. Flow rate controls material density; layer thickness helps to maintain the crack path and bonding area, and nozzle

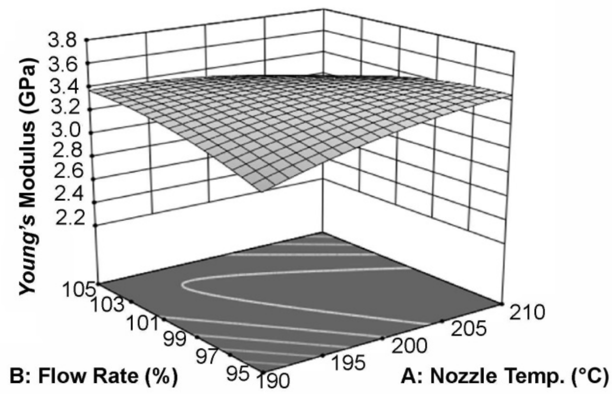

Fig. 4. Effect of material flow rate and nozzle temperature on *Young's* modulus (GPa)

Table 4

***ANOVA* results for *Young's* modulus (GPa)**

Source	*DF*	*Seq. SS*	*Adj. MS*	*F*	*P*
Layer thickness	2	1.6121	0.8061	6.86	0.005
Nozzle temperature	2	0.0285	0.0142	0.12	0.886
Flow rate	2	0.0100	0.0050	0.04	0.958
Error	20	2.3490	0.1175	–	–
Total	26	3.9996	–	–	–

temperature enhances molecular diffusion. The interaction of all factors at their optimal levels results in better toughness of the printed material. Fig. 5 shows that toughness increases with layer thickness and nozzle temperature. Table 5 shows that flow rate is the most significant parameter for toughness. Nozzle temperature and layer height show less effect on toughness. Multi-objective optimization of significant process parameters is needed to obtain the best printing parameters for the strength responses.

A higher grey relational grade (*GRG*) in the *GRA* optimization approach indicates a stronger link between the reference sequence and the comparison sequence (Table 6). With Rank 1, the ninth experimental run exhibits the highest *GRG* value. The multi-objective optimum set of printing parameters obtained during printing of *PLA* consists of layer thickness 0.1 mm, nozzle temperature 210 °C, and flow rate 105 % for the strength parameters tensile strength (MPa), toughness (J/mm^2), and *Young's* modulus (GPa) according to the multi-objective *GRA* method [19]. The dimensions of the talus bone developed in the laboratory using 3D printing are compared with the actual size of an adult patient's bone obtained from 3D scan data from hospitals and surgeons. A prototype of a real human bone was developed using the ideal set of

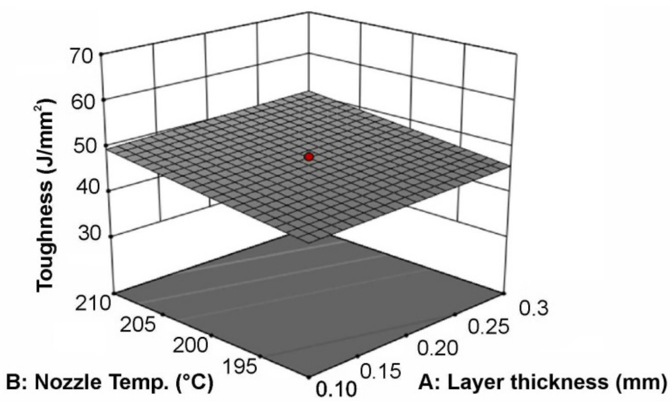

Fig. 5. Effect of nozzle temperature and layer thickness on toughness (J/mm^2)

Table 5

ANOVA results for toughness (J/mm²)

Source	*DF*	*Seq. SS*	*Adj. MS*	*F*	*P*
Layer thickness	2	26.74	13.37	2.92	0.077
Nozzle temperature	2	47.19	23.59	5.15	0.016
Flow rate	2	2155.63	1077.81	235.25	0.000
Error	20	91.63	4.58	–	–
Total	26	2321.19	–	–	–

Table 6

Grey relational coefficients and grey relational grade for response characteristics

Sr. No.	Norm. *TS*	Norm. Tough.	Norm. *YM*	GRC *TS*	GRC Tough.	GRC *YM*	*GRG*	Rank
1	0.033	0.000	0.100	0.357	0.340	0.333	0.3437	27
2	0.275	0.466	0.234	0.408	0.484	0.357	0.4162	25
3	0.625	0.833	0.458	0.571	0.749	0.394	0.5723	13
4	0.200	0.233	0.041	0.384	0.394	0.342	0.3741	26
5	0.775	0.433	0.183	0.689	0.468	0.379	0.5128	18
6	0.925	0.800	0.334	0.400	0.714	0.428	0.6716	5
7	0.750	0.334	0.667	0.667	0.428	0.479	0.5250	16
8	0.950	0.467	0.708	0.500	0.484	0.521	0.6382	8
9	1.000	0.800	0.908	1.000	0.714	0.844	0.8530*	1
10	0.000	0.000	0.750	0.334	0.334	0.600	0.4222	24
11	0.275	0.367	0.833	0.408	0.441	0.631	0.4936	20
12	0.525	0.900	0.850	0.512	0.833	0.666	0.6709	6
13	0.150	0.133	0.666	0.370	0.365	0.599	0.4454	23
14	0.325	0.467	0.833	0.425	0.484	0.749	0.5531	15
15	0.575	0.933	0.850	0.540	0.881	0.769	0.7306	3
16	0.225	0.234	0.708	0.392	0.394	0.631	0.4728	22
17	0.375	0.534	0.850	0.445	0.517	0.769	0.5802	12
18	0.625	1.000	0.900	0.571	1.000	0.833	0.8015	2
19	0.250	0.000	0.833	0.400	0.334	0.749	0.4983	19
20	0.450	0.400	0.983	0.476	0.454	0.967	0.6328	9
21	0.675	0.767	0.933	0.606	0.682	0.881	0.7233	4
22	0.275	0.066	0.875	0.408	0.348	0.800	0.5190	17
23	0.525	0.434	1.000	0.512	0.469	1.000	0.6605	7
24	0.725	0.834	0.408	0.645	0.750	0.457	0.6177	10
25	0.300	0.167	0.933	0.416	0.375	0.881	0.5579	14
26	0.625	0.334	0.334	0.571	0.428	0.428	0.4761	21
27	0.675	0.867	0.083	0.606	0.789	0.352	0.5828	11

printing settings in *AM*. A coordinate measuring machine (*CMM*) measured three coordinate dimensions: ***X*** = 51 mm (actual size: 50.8 mm), ***Y*** = 39 mm (actual size: 38.9 mm), and ***Z*** = 66 mm (actual size: 66.1 mm). As the dimensions are very close, the developed talus bone can be utilized as a prototype or pattern for the development of a talus bone using a biocompatible material such as *SS316L*.

It can be used for bone replacement during injuries or wear of the human bone [20]. Fig. 6 shows the actual view of the talus bone after development, and Fig. 7 shows the measurement of the adult talus bone under a *CMM*.

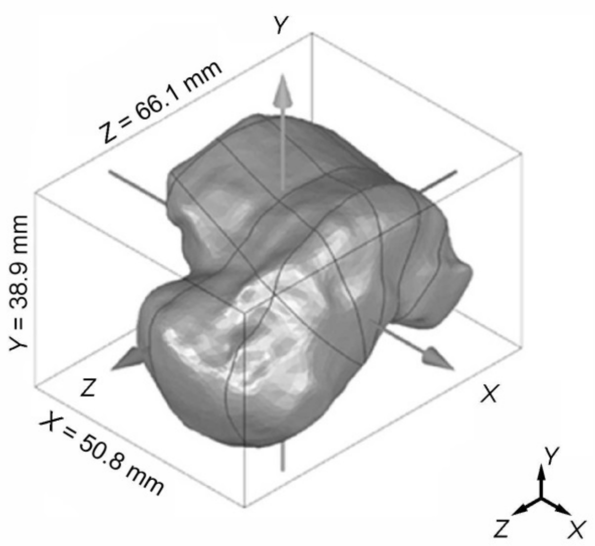

Fig. 6. Actual dimensions of the talus bone (adult patient)

Fig. 7. Dimensions of the talus bone measured using a coordinate measuring machine (*CMM*)

Conclusion

Additive manufacturing using fused deposition modeling was used for the development of a prototype of the human talus bone with *PLA* as the substrate. The important findings of the investigation are listed below:

– Tensile strength of the 3D-printed part increases from 21 MPa to 42 MPa with an increase in layer thickness from 0.1 to 0.3 mm, but a further increase in layer thickness (0.2 mm to 0.3 mm) shows a downward trend in tensile strength. *ANOVA* analysis for tensile strength (MPa) shows that flow rate is the most significant process parameter, followed by layer height and nozzle temperature.

– An increase in the flow rate of PLA from 95% to 100% results in less porosity and fewer voids, with better fusion of layers, but a further increase in flow rate (100% to 105%) leads to a bulging effect with internal stresses and microcracks during solidification, which results in poor surface quality. *ANOVA* analysis shows that layer height is the most prominent parameter for *Young's* modulus. Nozzle temperature and flow rate have less effect on the *Young's* modulus of the printed part.

– It is observed that with an increase in nozzle temperature from 190 °C to 210 °C, *Young's* modulus values show an increasing trend because strong thermal contact allows the layer to fuse fully. *Young's* modulus shows an increasing trend with increasing nozzle temperature. However, an increase in flow rate and layer thickness leads to the creation of voids, gaps, and incomplete fusion between deposited layers. *Young's* modulus shows a decreasing trend with increasing flow rate and layer thickness. *ANOVA* shows that flow rate is the most significant parameter for toughness. Nozzle temperature and layer thickness show less effect on toughness.

– The multi-objective optimum set of printing parameters obtained during printing of *PLA* consists of layer thickness 0.1 mm, nozzle temperature 210 °C, and flow rate 105% for the strength parameters tensile strength (MPa), toughness (J/mm^2), and *Young's* modulus (GPa) according to the multi-objective *GRA* method.

– A prototype of a real human bone was developed using the ideal set of printing settings in *AM*. A coordinate measuring machine measured three coordinate dimensions: ***X*** = 51 mm (actual size: 50.8 mm), ***Y*** = 39 mm (actual size: 38.9 mm), and ***Z*** = 66 mm (actual size: 66.1 mm). As the dimensions are very close, the developed talus bone can be utilized as a prototype or pattern for the development of a talus bone using a biocompatible material such as *SS316L*.

This approach will be helpful for further converting the polymer prototype into a metallic implant in the era of bioengineering. 3D additive manufacturing has been proven to be a promising manufacturing tool in the biomedical field.

References

1. Chunxu L., Pisignano D., Zhao Y., Xue J. Advances in medical applications of additive manufacturing. *Engineering*, 2020, vol. 6 (11), pp. 1222–1231. DOI: 10.1016/j.eng.2020.02.018.

2. Kirichek A.V., Solovyev D.L., Yashin A.V., Silantyev S.A., Aborkin A.V., Novikov M.A. Issledovanie anizotropii svoistv sintezirovannykh metallicheskikh materialov WAAM-metodom [Anisotropy of properties in metal materials fabricated by wire arc additive manufacturing (WAAM)]. *Obrabotka metallov (tekhnologiya, oborudovanie, instrumenty) = Metal Working and Material Science*, 2025, vol. 27, no. 4, pp. 206–220. DOI: 10.17212/1994-6309-2025-27.4-206-220.

3. Rouf S., Malik A., Raina A., Haq M.I.U., Naveed N., Zolfagharian A., Bodaghi M. Functionally graded additive manufacturing for orthopaedic applications. *Journal of Orthopaedics*, 2022, vol. 33, pp. 70–80. DOI: 10.1016/j.jor.2022.06.013.

4. Gupta K., Meena K. Artificial bone scaffolds and bone joints by additive manufacturing: a review. *Bioprinting*, 2023, vol. 31, p. e00268. DOI: 10.1016/j.bprint.2023.e00268.

5. Farazin A., Zhang C., Gheisizadeh A., Shahbazi A. 3D bio-printing for use as bone replacement tissues: a review of biomedical application. *Biomedical Engineering Advances*, 2023, vol. 5, p. 100075. DOI: 10.1016/j.bea.2023.100075.

6. Myers D., Abdel-Wahab A., Hafeez F., Kovacev N., Essa K. Optimisation of the additive manufacturing parameters of polylactic acid (PLA) cellular structures for biomedical applications. *Journal of the Mechanical Behavior of Biomedical Materials*, 2022, vol. 136, p. 105447. DOI: 10.1016/j.jmbbm.2022.105447.

7. Bakhshi R., Mohammadi-Zerankeshi M., Mehrabi-Dehdezi M., Alizadeh R., Labbaf S., Abachi P. Additive manufacturing of PLA-Mg composite scaffolds for hard tissue engineering applications. *Journal of the Mechanical Behavior of Biomedical Materials*, 2023, vol. 138, p. 105655. DOI: 10.1016/j.jmbbm.2023.105655.

8. Settia M., Ginestra P. Additive manufacturing for orthopaedic applications: case study on market impact. *Procedia Computer Science*, 2023, vol. 217, pp. 737–745. DOI: 10.1016/j.procs.2022.12.270.

9. Liu G., Lu X., Zhang X., Zhao Y., Yi S., Xu J., Feng C., Zhou Z., Wang P., Chen Z., He Y., Chen S., Liu P., Zuo J., Dai Y., Wu J., Liu S., Lu J. 3D/4D additive-subtractive manufacturing of heterogeneous ceramics. *Journal of Materials Science & Technology*, 2024, vol. 201, pp. 210–221. DOI: 10.1016/j.jmst.2024.02.069.

10. Chen D., Chen Y. Optimization parameters for PLA through additive manufacturing: taking mixed shapes as an example. *Applied Sciences*, 2024, vol. 14 (21), p. 10035. DOI: 10.3390/app142110035.

11. Almansoori K., Pervaiz S. Effect of layer height, print speed and cell geometry on mechanical properties of marble PLA based 3D printed parts. *Smart Materials in Manufacturing*, 2023, vol. 1, p. 100023. DOI: 10.1016/j.smmf.2023.100023.

12. Raja S., Prakash A., Agrawal P., Patil P., Rey T., Capangpangan Y., Mulugeta S., Wotango T. Optimization of 3D printing process parameters of polylactic acid filament based on the mechanical test. *International Journal of Chemical Engineering*, 2022, vol. 2022, p. 5830869. DOI: 10.1155/2022/5830869.

13. Bilir F., Turker K., Saadet T., Ahmet G., Kilinc C. Optimization of 3D printing parameters for enhanced tensile properties in continuous carbon fiber reinforced PLA composites. *Materials Research Express*, 2025, vol. 12 (4), p. 045302. DOI: 10.1088/2053-1591/adc5cc.

14. Dadashi A. Optimization of 3D printing parameters in polylactic acid bio-metamaterial under cyclic bending loading considering fracture features. *Heliyon*, 2024, vol. 10 (4), p. e26357. DOI: 10.1016/j.heliyon.2024.e26357.

15. Kechagias J., Zaoutsos S. Optimization window of printing parameters for specific strength and energy consumption in PEEK additive manufacturing. *Materials and Manufacturing Processes*, 2026, vol. 41 (2), pp. 229–236. DOI: 10.1080/10426914.2026.2613641.

16. Chate G., Deshpande A. Optimisation for geometrical dimension of a product using 3D printer based on fused deposition modelling. *International Journal of Additive and Subtractive Materials Manufacturing*, 2017, vol. 1 (2), pp. 133–144. DOI: 10.1504/IJASMM.2017.088201.

17. Ilyushkin D.A., Soldatov V.G., Petrakov O.V., Kotlyarova I.A. K voprosu vybora i optimizatsii parametrov nepreryvnoi lazernoi svarki chuguna [On the issue of selecting and optimizing parameters of continuous laser welding of cast iron]. *Obrabotka metallov (tekhnologiya, oborudovanie, instrumenty) = Metal Working and Material Science*, 2021, vol. 23, no. 3, pp. 20–30. DOI: 10.17212/1994-6309-2021-23.3-20-30.

18. Agrawal D., Kamble D. Optimization of photochemical machining process parameters for manufacturing microfluidic channel. *Materials and Manufacturing Processes*, 2018, vol. 34 (1), pp. 1–7. DOI: 10.1080/10426914.2018.1512115.

19. Karthikeyan A., Prabhu L., Khan T., Sebaey T. Effect of process variables on Ultimaker 2+ 3D FDM printed tough PLA parts. *Materials and Manufacturing Processes*, 2025, vol. 40 (3), pp. 402–414. DOI: 10.1080/10426914.2024.2425622.

20. Wolf C., Juchem D., Koster A., Pilloy W. Generation of customized bone implants from CT scans using FEA and AM. *Materials*, 2024, vol. 17 (17), p. 4241. DOI: 10.3390/ma17174241.

Conflicts of Interest

The authors declare no conflict of interest.